

Autoconfocal transmission microscopy based on two-photon-induced photocurrent of Si photodiodes

Chulmin Joo,* Chun Zhan, Qing Li, and Siavash Yazdanfar

GE Global Research, One Research Circle, Niskayuna, New York 12309, USA

*Corresponding author: joo@ge.com

Received August 14, 2009; revised November 30, 2009; accepted December 1, 2009;
posted December 10, 2009 (Doc. ID 115754); published December 24, 2009

We describe a simple, self-aligned confocal transmission microscopy technique based on two-photon-induced photocurrents of silicon photodiodes. Silicon detectors produce photocurrents in quadratic dependence on incident intensity under the pulsed illumination of light with wavelengths longer than $1.2 \mu\text{m}$. We exploit this nonlinear process to reject out-of-focus background and perform depth-sectioning microscopic imaging. We demonstrate a comparable background rejection capability of the technique to linear confocal detection and present three-dimensional imaging in biological specimens. © 2009 Optical Society of America
OCIS codes: 180.0180, 180.1790, 180.4315, 180.5810.

Laser-scanning confocal microscopy (LSCM) is capable of producing high-contrast, high-resolution images of biological and material specimens with optical sectioning capability. The improved image contrast and depth sectioning in LSCM is enabled by a physical pinhole placed in front of the image plane, which allows in-focus portion of light to be measured while rejecting stray light from out-of-focus background [1]. LSCM can be implemented either in reflection or transmission modes. In the reflection or epi-detection mode, the light collected from the specimen is typically descanned to pass through a stationary pinhole and measured with a detector. However, this configuration is not preferable for scattering-based imaging of weakly scattering biological specimens such as cells and thin tissues, as the scattered light from these samples is predominantly in the forward direction. To obtain images with high contrast, therefore, highly sensitive detectors such as photomultiplier tubes (PMTs) or avalanche photodiodes are employed. In the transmission mode, the light transmitted through the specimen has higher intensity, alleviating a need for highly sensitive detectors. Yet, to acquire images, a dedicated mechanism is required to descann the beam or to move the pinhole synchronously with the illumination beam. Previous researchers have noted and addressed this issue by presenting a self-aligned confocal transmission microscope based on a second-harmonic generation (SHG) crystal in the detection path [2,3]. In this technique, termed autoconfocal microscopy (ACM), light transmitted through the specimen is collected and re-focused onto the SHG crystal. As the generated SHG signal scales quadratically with incident light intensity over the entire crystal plane, the crystal serves as a self-aligned virtual pinhole for out-of-focus background rejection. Lim *et al.* recently introduced an alternative scheme employing thermionic emission of a PMT photocathode [4]. Since the number of electrons generated by the light-induced heat at the PMT photocathode is nonlinear in incident intensity, the PMT photocathode can act as a virtual pinhole for autoconfocal imaging. In contrast to other autoconfocal techniques, this method does not require a femtosecond

pulsed laser to induce a nonlinear response in the detector and can be achieved with a simple CW laser.

Here, we present another strategy for ACM based on two-photon-induced photocurrents of a silicon photodiode (Si-PD). Two-photon-induced photocurrents in solid-state devices have been observed and extensively used in many applications, including high-resolution defect imaging of integrated circuits [5] and light-emitting diodes [6], and pulse-width measurement of ultrafast pulses [7]. In our case, we employ the nonlinear response of the Si-PD to a $\sim 1.55 \mu\text{m}$ fiber-based femtosecond laser [7] for both virtual pinhole and detector, eliminating the need for a physical pinhole for confocal imaging. A significant advantage of this technique is that the desired nonlinear absorption and the transformation of light into the electric current are combined into a single, readily available photodiode, enabling a simple and efficient implementation for ACM. Moreover, the use of a near-IR fiber laser is significantly cheaper than imaging with Ti:sapphire femtosecond lasers and provides a deeper imaging depth due to the longer wavelength.

We first examined a response of Si-PD under focused light illumination at $\sim 1.55 \mu\text{m}$. Light from an erbium-doped fiber-based laser (Mercury 1000, Polar-Onyx Inc., California) with a pulse duration of ~ 100 fs and repetition rate of ~ 50 MHz was focused onto an amplified Si-PD (PDA55, Thorlabs Inc., New Jersey) using an average incident optical power of ~ 30 mW and beam diameter of $\sim 10 \mu\text{m}$. The Si-PD output was measured under continuous (CW) and pulsed wave (PW) illumination [Fig. 1(a)] by adjusting the mode-locking of the laser with polarization controllers in the fiber ring cavity. For the CW case, no signal was observed on the detector, since $\sim 1.55 \mu\text{m}$ light energy is below the bandgap of Si. However, PW illumination resulted in a remarkable signal increase. We examined the output signal as a function of the incident optical power for the PW case, and found that the signal exhibited a quadratic dependence on the incident optical power [Fig. 1(b)]. The output signal was larger than the dark current if the incident power exceeded ~ 0.05 mW. In principle,

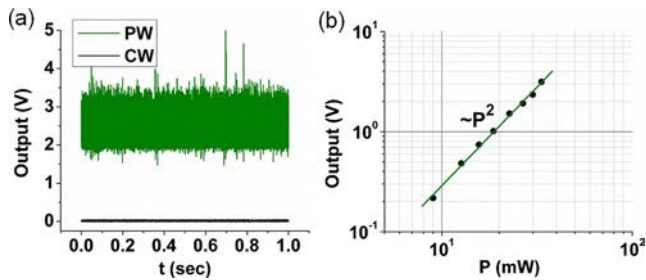


Fig. 1. (Color online) Si-PD output was measured under focused illumination of an $\sim 1.55 \mu\text{m}$ light. CW illumination did not generate a signal, as the incident light energy was below the Si bandgap. However, under PW illumination, nonlinear absorption in Si generated appreciable photocurrents, which exhibited a quadratic dependence on incident intensity.

several processes could give rise to the observed nonlinear detector response, such as thermionic emission [4], SHG [2,3], and two-photon absorption. However, for a given average power, the detector response due to thermionic emission would be equivalent for the CW and PW cases. Therefore, it can be concluded that thermionic emission is not a main contributor to the detected signal. SHG is also excluded, because the signal level was independent of the polarization state of the incident optical beam.

Having thus confirmed two-photon absorption in the Si-PD, we implemented the microscope using the same light source, as depicted in Fig. 2. Objectives with NAs of 0.8 and 0.6 (Plan-Apochromat 0.8/20 \times , LD Achroplan 0.6/40 \times , Zeiss) were used as focusing and detection lenses, respectively, to achieve high transmission and low aberration at the employed wavelength ($\sim 1.55 \mu\text{m}$). The transmitted light through the specimen was focused onto the Si-PD via the focusing lens (focal length $\sim 25 \text{ mm}$) with a diffraction-limited beam diameter of $\sim 10 \mu\text{m}$. The confocal parameter at the detector plane was $\sim 400 \mu\text{m}$, which is larger than the typical thickness of the depletion layer of Si-PDs.

To assess the depth discrimination capability of the ACM, we examined the Si-PD output by scanning the detector through the focus of the focusing lens in the absence of a specimen (Fig. 3). Even though the total power at any axial position was constant, the Si-PD output dropped as the detector moved away from the

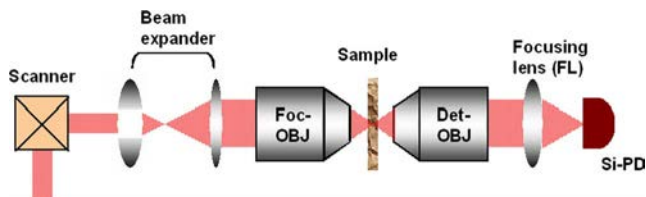


Fig. 2. (Color online) Schematic of ACM. A beam from a $\sim 1.55 \mu\text{m}$ femtosecond fiber laser was employed as a light source. The light transmitted through the sample was focused onto and detected by the Si-PD. Foc-OBJ and Det-OBJ are microscope objectives for focusing and detection path.

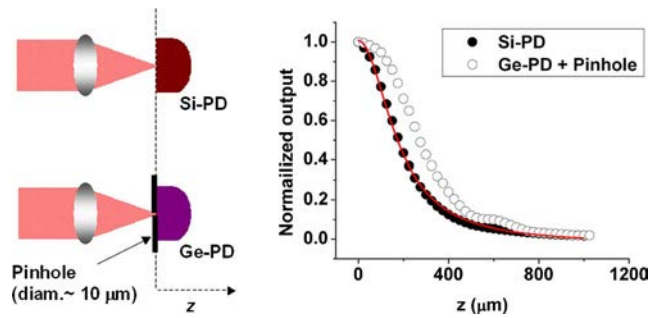


Fig. 3. (Color online) Virtual pinhole effect exhibited by nonlinear response of Si-PD was compared with that of linear confocal detection (Ge-PD+10 μm diameter pinhole). Scanning both detectors through focus revealed a comparable axial response between the Si-PD and linear confocal detection. The solid curve indicates a fit to $\sim 1/z^2$.

focal position. In order to compare the response with that for conventional linear confocal detection, a linear confocal detector composed of a germanium photodiode (Ge-PD; DET50B, Thorlabs Inc.) and a physical pinhole was placed at the detector plane. The Ge-PD has a peak responsivity at $\sim 1.55 \mu\text{m}$ and exhibits a linear relationship with incident intensity. We chose the size of the physical pinhole as $\sim 10 \mu\text{m}$ in order to match the diffraction-limited $\sim 10 \mu\text{m}$ beam spot size on the Si-PD for the autoconfocal case. The signal for the linear confocal detection produced a similar response, demonstrating that Si-PD based ACM provides a depth sectioning capability comparable to that of linear confocal detection with a $\sim 10 \mu\text{m}$ aperture. As in conventional confocal microscopy, the effective pinhole size in ACM can be found simply by projecting the pinhole size back onto the sample plane [8–10]. We found the effective virtual pinhole size at the sample plane as $\sim 1.6 \mu\text{m}$ in our case, which corresponds to the FWHM axial resolution of $\sim 3.8 \mu\text{m}$ based on the analysis described in [8,9]. We experimentally verified the axial resolution of the ACM by obtaining through-focus images of a phantom comprising polystyrene microbeads (Duke Standards, 4009A, nominal diameter $\sim 1 \mu\text{m}$) embedded in agarose gel. The measured FWHM axial resolution of the system ($\sim 4.6 \mu\text{m}$) agreed with the theoretical estimation to within $\sim 21\%$.

The improved image contrast and rejection of out-of-focus background by ACM was further assessed by imaging $\sim 20\text{-}\mu\text{m}$ -thick fixed rat retina. Figures 4(a) and 4(b) show the images obtained with the Si-PD based nonlinear detection and Ge-PD based linear detection, i.e., the detector with no pinhole, respectively. The pixel dwell time was $100 \mu\text{s}$. The optical power at the sample was $\sim 10 \text{ mW}$. While vascular and morphological structures were visible in both images, the out-of-focus background rejection capability in ACM resulted in a much higher contrast and more detailed morphological features than in the image taken by the Ge-PD based linear detection. More quantitatively, the image contrast $C = (I_{\text{max}} - I_{\text{min}}) / (I_{\text{max}} + I_{\text{min}})$ was found to be 0.75 for ACM and 0.20 for the linear detection, showing a remarkable image contrast improvement by ACM. In order to

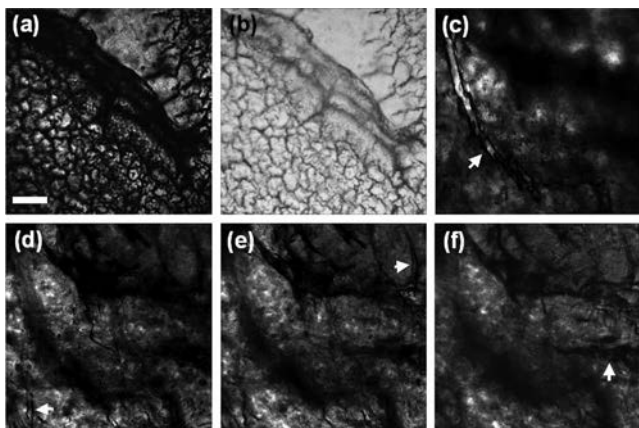


Fig. 4. (a)–(b) Images of a fixed rat retina tissue recorded with Si-PD based ACM and Ge-PD based linear detection, respectively. Note the improved image contrast provided by Si-PD based nonlinear detection. (c)–(f) Si-PD based ACM images of fixed rat choroid tissue at tissue surface and 20, 40, 60 μm below the tissue surface, respectively. Vascular structures and epithelium are clearly visible at each depth with high contrast. The scale bar represents 50 μm .

implement conventional pinhole-based confocal detection in transmission, a dedicated mechanism would be required to descan the beam in the detection path, or to move the pinhole synchronously with the laser beam.

We next performed ACM imaging on $\sim 80\text{-}\mu\text{m}$ -thick fixed rat choroid tissue by scanning the sample along the optical axis to demonstrate three-dimensional imaging capability. The power at the specimen was $\sim 10\text{ mW}$. The representative images at the tissue surface and in $\sim 20\text{ }\mu\text{m}$ steps below the surface are shown in Figs. 4(c), 4(d), and 4(f). The distribution of vascular structures (indicated by solid arrows) and epithelium at different depths is clearly visible while high image contrast is maintained.

A notable feature of Si-PD based ACM is its simplicity, as a single Si-PD itself serves as both self-aligned virtual pinhole and detector. While it requires a pulsed laser at wavelengths longer than $1.2\text{ }\mu\text{m}$ for operation, it provides a deeper imaging depth compared to visible wavelengths and can be easily integrated with nonlinear microscopy techniques, such as two-photon fluorescence microscopy (2PM) of near-IR dyes [11] and SHG microscopy [12]. The image contrast of ACM is based on scattering and absorption properties of the sample, providing structural and morphological information without exogenous contrast agents. It thus would be complementary to 2PM and SHG imaging, which visualize

only the structures that exhibit fluorescence or that lack a center of symmetry, respectively.

The three-dimensional spatial resolution of ACM is determined by both the focusing beam spot size and the effective virtual pinhole size, as in conventional pinhole-based confocal imaging systems [2,10]. The effective virtual pinhole size in ACM can be approximated as the diffraction-limited beam spot size through the detection objective, inversely proportional to its numerical aperture ($\sim 1/\text{NA}_{\text{Det-Obj}}$) [10]. The smaller virtual pinhole achieved by a higher NA detection objective thus leads to higher spatial resolution and better depth sectioning without compromising the signal strength [10].

In summary, a cheap and simple scheme for autoconfocal transmission microscopy was demonstrated. The self-aligned virtual pinhole was achieved by a single large-area silicon photodiode that generates photocurrent in quadratic dependence on incident intensity at $\sim 1.55\text{ }\mu\text{m}$ pulsed illumination. The Si-PD based ACM demonstrated background rejection comparable to that of linear confocal detection. Depth-sectioning capability of the technique was also presented by showing the images of fixed retina and choroid tissues.

This research was supported by research grants from National Institutes of Health (NIH) (R21/R33 CA123537).

References

1. T. Wilson and C. J. R. Sheppard, *Theory and Practice of Scanning Optical Microscopy* (Academic, 1984).
2. T. Pons and J. Mertz, *J. Opt. Soc. Am. B* **21**, 1486 (2004).
3. C. Yang and J. Mertz, *Opt. Lett.* **28**, 224 (2003).
4. D. Lim, K. K. Chu, and J. Mertz, *Opt. Lett.* **33**, 1345 (2008).
5. C. Xu and W. Denk, *Appl. Phys. Lett.* **71**, 2578 (1997).
6. F.-J. Kao, M.-K. Huang, Y.-S. Wang, S.-L. Huang, M.-K. Lee, and C.-K. Sun, *Opt. Lett.* **24**, 1407 (1999).
7. L. P. Barry, P. G. Bollond, J. M. Dudley, J. D. Harvey, and R. Leonhardt, *IEEE Electronics Letters* **32**, 1992 (1996).
8. T. Wilson and A. R. Carlini, *Opt. Lett.* **12**, 227 (1987).
9. T. Wilson, in *Handbook of Biological Confocal Microscopy*, J. B. Pawley, ed. (Plenum, 1995).
10. K. K. Chu, R. Yi, and J. Mertz, *Opt. Express* **15**, 2476 (2007).
11. S. Yazdanfar, C. Joo, C. Zhan, M. Y. Berezin, W. J. Akers, and S. Achilefu, *Opt. Express*, submitted for publication.
12. M. Han, G. Giese, and J. Bille, *Opt. Express* **13**, 5791 (2005).